nature climate change

SUPPLEMENTARY INFORMATION
https://doi.org/10.1038/s41558-019-0531-8

In the format provided by the authors and unedited.

Persistent acceleration in global sea-level rise since the 1960s

Sönke Dangendorf[1,2*], Carling Hay[3], Francisco M. Calafat[4], Marta Marcos[5], Christopher G. Piecuch[6], Kevin Berk[7] and Jürgen Jensen[1]

[1]Research Institute for Water and Environment, University of Siegen, Siegen, Germany. [2]Department of Ocean, Earth and Atmospheric Sciences, Old Dominion University, Norfolk, VA, USA. [3]Department of Earth and Environmental Sciences, Boston College, Chestnut Hill, MA, USA. [4]National Oceanography Centre, Liverpool, UK. [5]IMEDEA (UIB-CSIC), Esporles, Spain. [6]Woods Hole Oceanographic Institution, Woods Hole, MA, USA. [7]Stochastik und Quantitative Methoden der Wirtschaftswissenschaften, University of Siegen, Siegen, Germany. *e-mail: soenke.dangendorf@uni-siegen.de

Persistent acceleration in global sea-level rise since the 1960s

Sönke Dangendorf[1,2], Carling Hay[3], Francisco M. Calafat[4], Marta Marcos[5], Christopher G. Piecuch[6], Kevin Berk[7], and Jürgen Jensen[1]

[1]Research Institute for Water and Environment, University of Siegen, Paul-Bonatz-Str. 9-11, 57076, Siegen, Germany.

[2]Department of Ocean, Earth and Atmospheric Sciences, Old Dominion University, 4600 Elkhorn Avenue, Norfolk, VA23529, USA

E-mail : soenke.dangendorf@uni-siegen.de

[3]Boston College, Devlin Hall 323, Chestnut Hill, MA02467, USA

[4]National Oceanography Centre, Joseph Proudman Building, 6 Brownlow Street, Liverpool, L35DA, UK

[5]IMEDEA (UIB-CSIC), Miquel Marques 21, E-07190, Esporles, Spain

[6]Woods Hole Oceanographic Institution, MS#21, Woods Hole, MA 02543-1050, USA

[7]University of Siegen, Emmy-Noether-Campus, Walter-Flex Str. 3, 57072, Siegen, Germany

Supplementary Figures

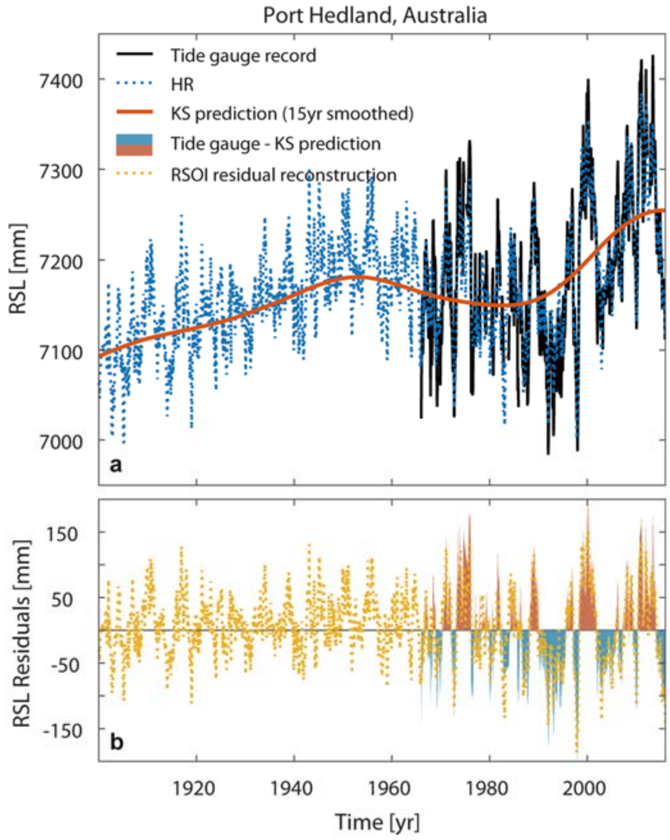

Fig. S1 | Principle of the HR at an individual tide gauge record. a Shown is the initially available PSMSL tide gauge record at Port Hedland, Australia, the corresponding smoothed (15 years) KS prediction and the final HR. **b** Residuals of the difference between the original PSMSL tide gauge record and the smoothed KS prediction (both shown in **a**) and their corresponding RSOI reconstruction without consideration of EOF0.

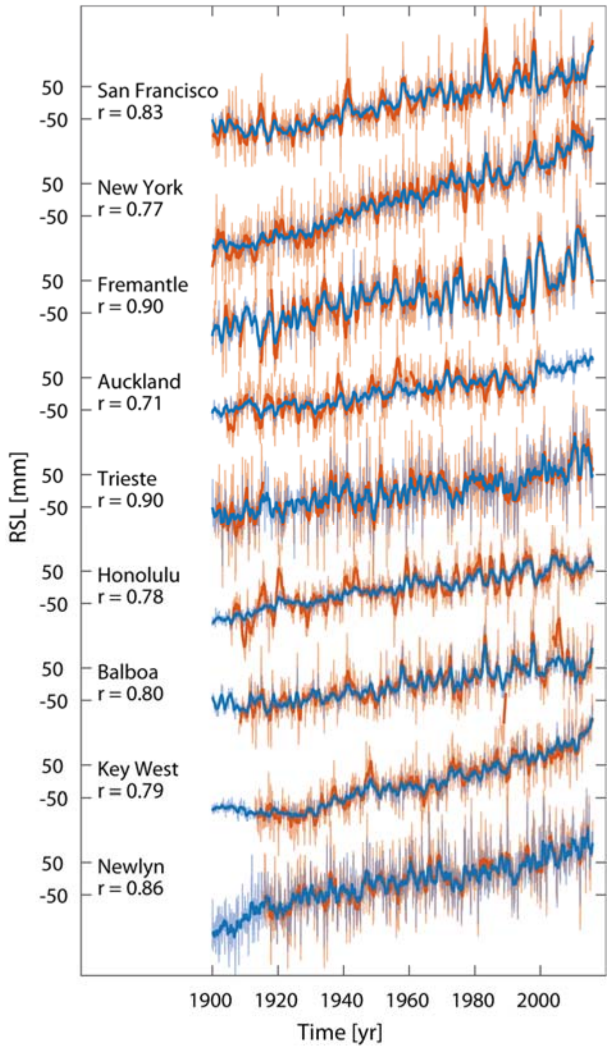

Fig. S2 | Comparison of the HR with individual tide gauge records. Shown are 9 long and widely used tide gauge records (red) and the corresponding HR (blue). Thin and thick lines mark monthly and annual time series, respectively. Also shown are the correlations between the de-trended annual time series at each site.

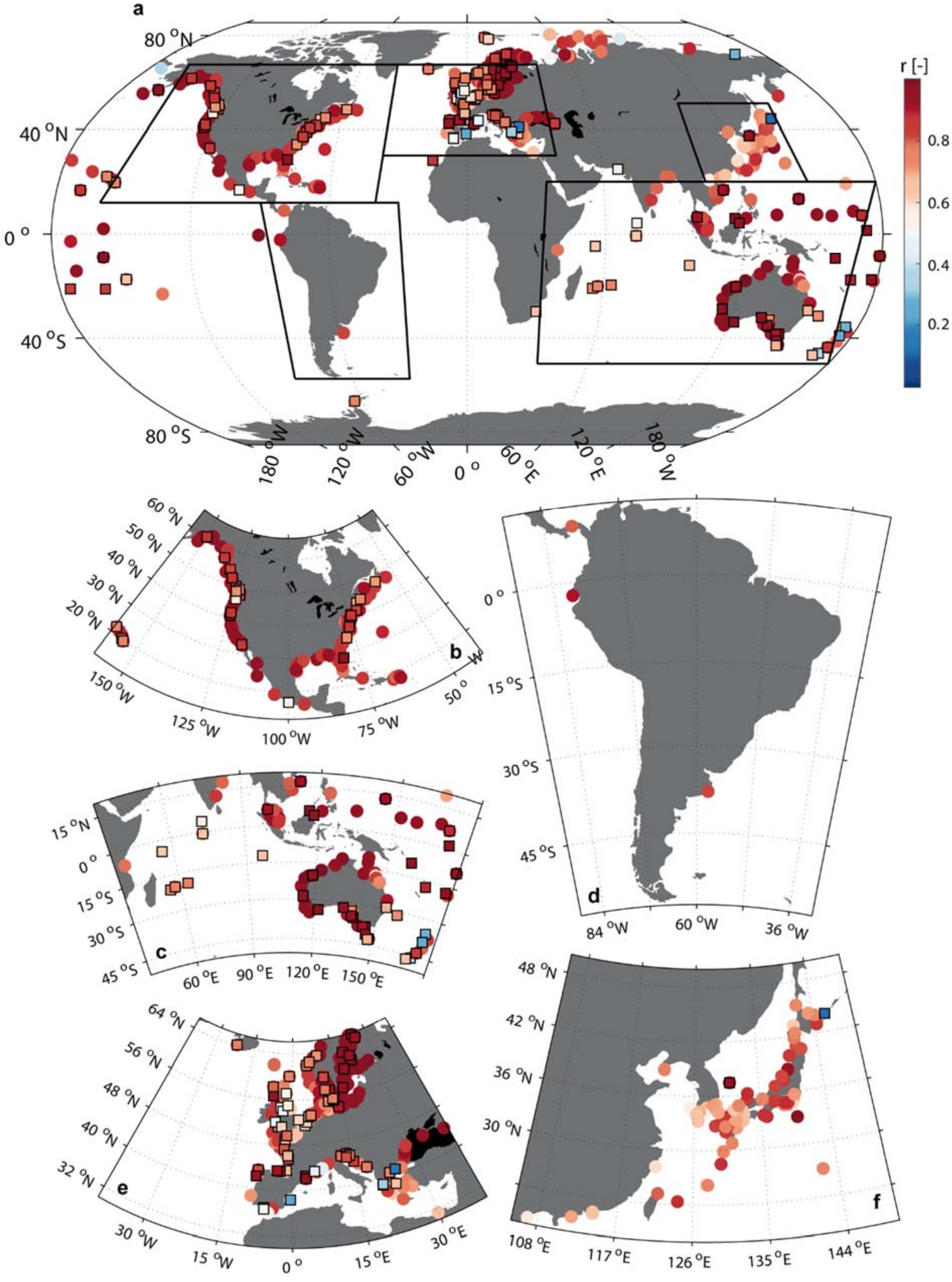

Fig. S3 | Comparison between the HR and individual tide gauge sites. Shown are the correlations between de-trended annual tide gauge records and the corresponding HR time series for sites used in the reconstruction (circles) and independent validation sites (black colored squares) globally (**a**), and zooms of 5 sub-regions (**b**-**f**) shown as black boxes in (**a**).

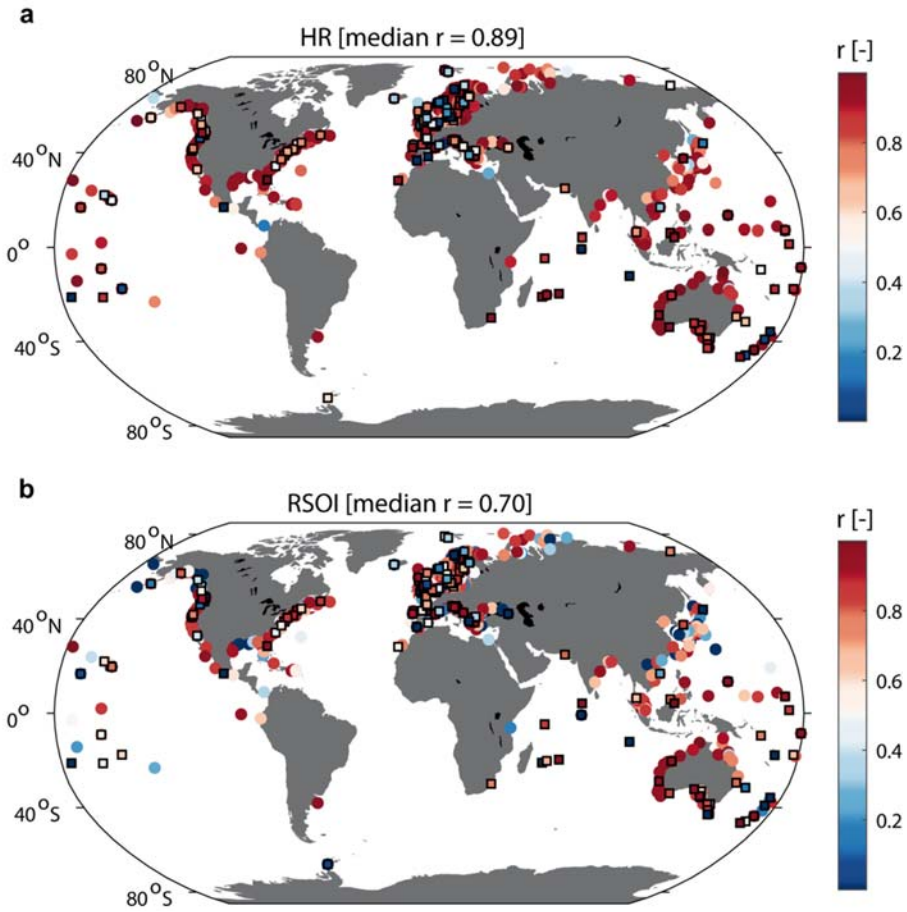

Fig. S4 | Decadal correlations of the HR and RSOI with individual tide gauges. Shown are the correlations between de-trended and decadally smoothed time series of individual tide gauge records and the HR (**a**) as well as individual tide gauge records and the RSOI (**b**). As in **Fig. S3**, sites used in the reconstruction are marked as colored circles, while independent validation sites are shown as black colored squares.

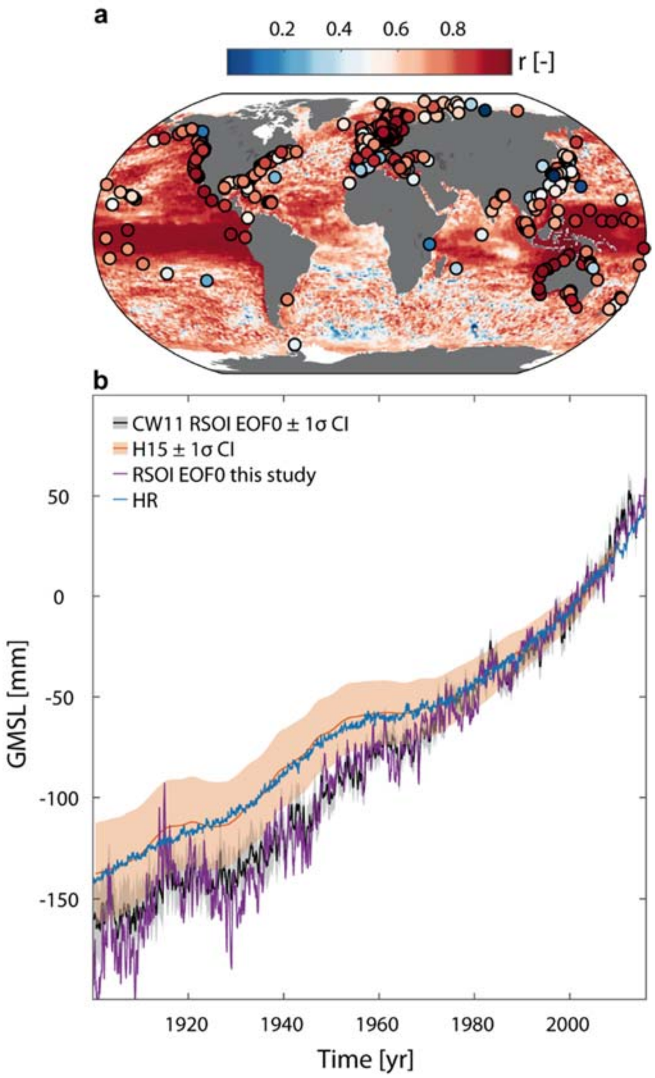

Fig. S5 | Comparison of the HR to former reconstructions and performance of the RSOI using EOF0. a, Correlation between the RSOI reconstruction with EOF0 similar to ref. 10 in the main text and satellite altimetry during 1993-2015 (shading) and tide gauges (black circles) during their overlapping periods. Correlations have been calculated based on annual and de-trended time series. The plot can directly be compared to the map based on the HR shown in **Fig. 1**. **b** Shown are two former reconstructions from ref. 10 (CW11) and ref. 12 (H15), the RSOI using the EOF0 similar to ref. 10 but using the 479 sites from the present study (applying the GIA correction from ref. 57) and the HR. Shadings represent the 1σ uncertainties from the two former studies.

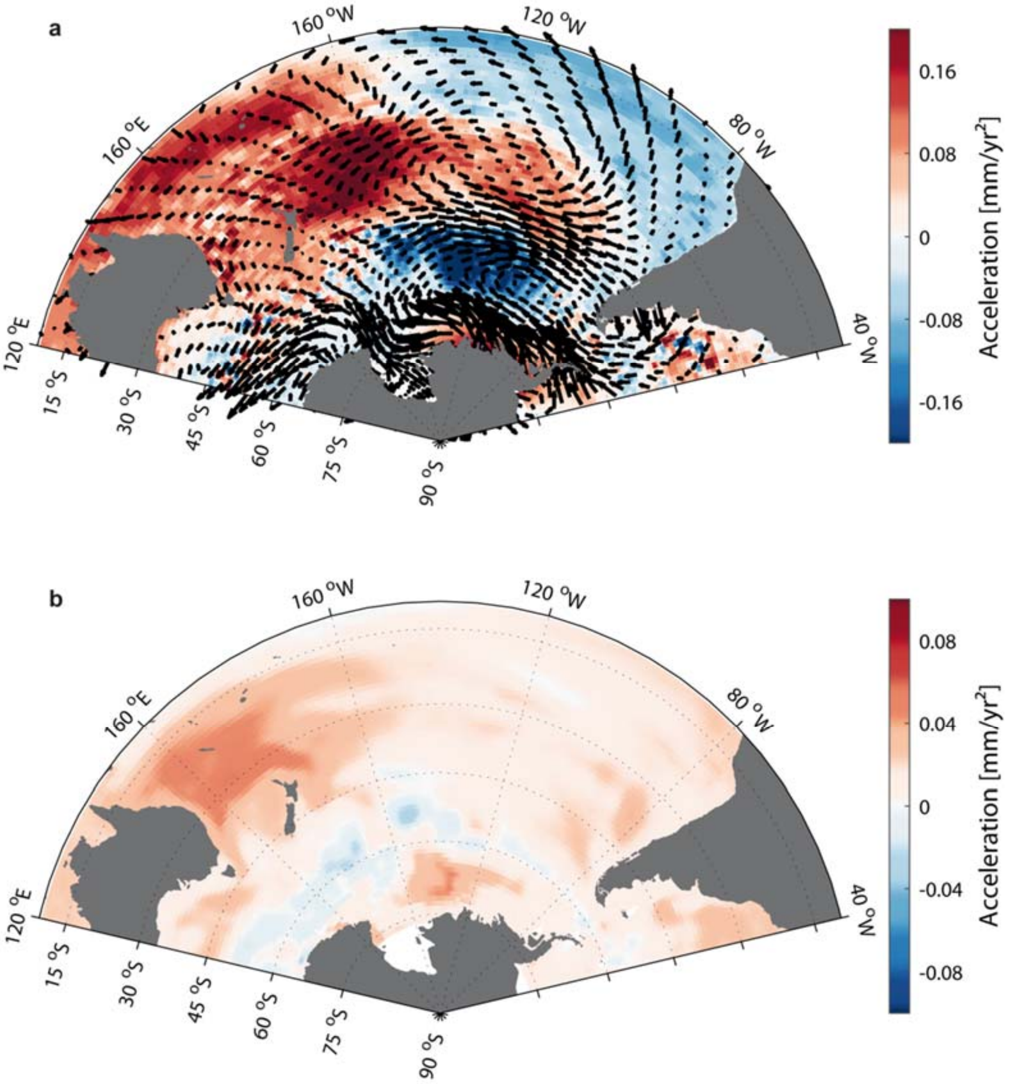

Fig. S6 | South Pacific sea-level acceleration in the HR, CMIP5 models, and wind stress during 1968-2015. Shown are acceleration coefficients determined with a quadratic Ordinary Least Squares fit for (**a**) dynamic sea level from the HR (after removing the component of GIA and present day mass contributions, and therefore jointly determined by ocean density and circulation) and surface wind stress from the 20^{th} century reanalysis (black arrows), as well as (**b**) the ensemble average of the dynamic component from CMIP5 climate model runs from Supplementary ref. 1. Note the different labelling of both axes.

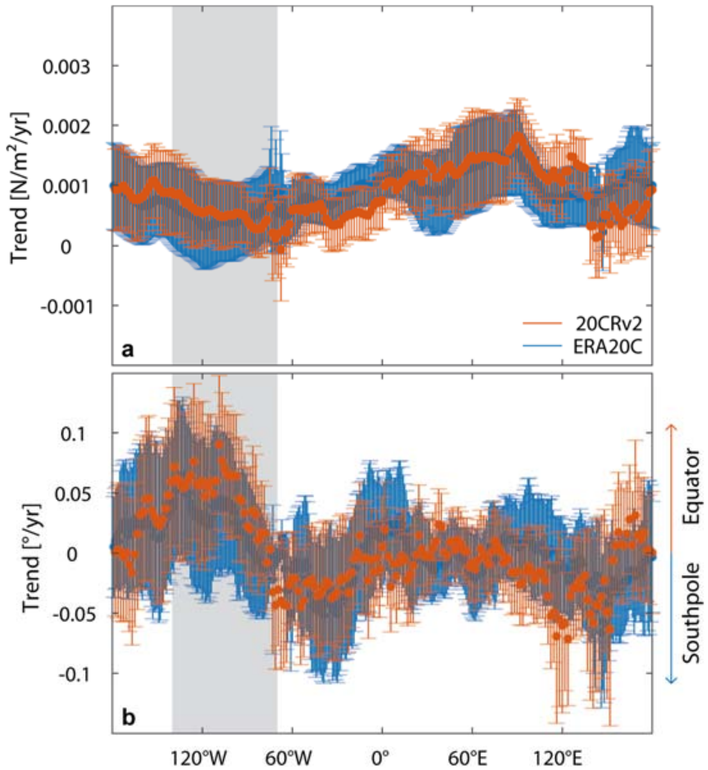

Fig. S7 | Trends in the Southern Hemispheric Westerlies intensity and position per longitude. Shown are linear trends over the period 1967-2010 (the acceleration plateau) for the intensity (**a**) and the position (**b**) of Southern Hemispheric Westerlies in two different reanalysis products (20CRv2 and ERA20C) calculated following the algorithm by ref. 39. The error bars correspond to the 2σ uncertainties, while the grey shading marks the area in which a latitudinal shift towards the equator has been observed.

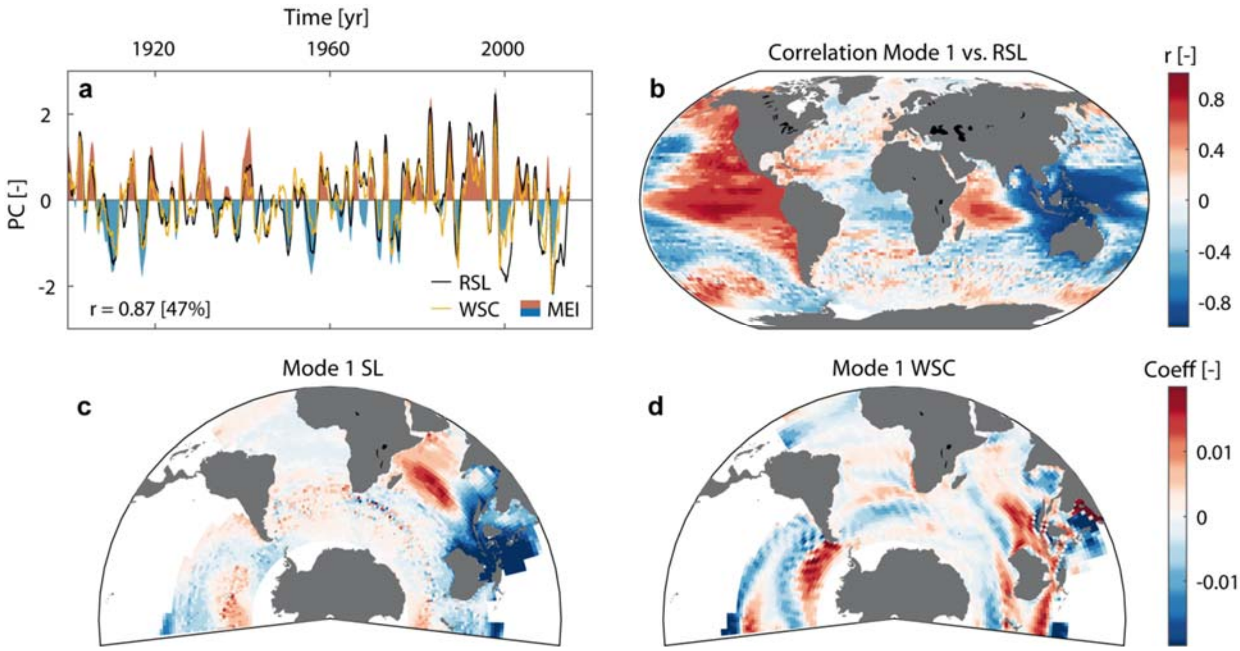

Fig. S8 | Sea level and Southern Hemispheric Wind forcing. Shown are, complementary to **Fig. 4** in the main text, the results of the MCA between detrended dynamic sea level (SL, corrected for the contributions from GIA and present day mass contributions, and therefore jointly determined by ocean density and circulation) and WSC (from the 20th century reanalysis) over Regions 1 (South Atlantic) and 2 (Indo-Pacific) for the first EOF. **a**, First coupled PC (explaining 47% of their squared covariance) from SL and WSC (smoothed with a moving average of 12 months). Also shown is the smoothed multivariate ENSO index (MEIc), which is significantly correlated with the PCs from SL (r = 0.83) and WSC (r = 0.80). **b**, Correlation map between the coupled SL PC1 and SL at each grid point around the globe. **c**, **d**, The corresponding EOF modes for SL and WSC. The figure illustrates the important role of ENSO on inter-annual wind-driven SL variations over the entire ocean and in particular the Southern Hemipshere and tropics. It also demonstrates that, although with less magnitude than PCs 2 and 3, PC1 has additionally contributed to the positive trends in the South Pacific over the recent decades due to an accumulation of La Nina events during that period.

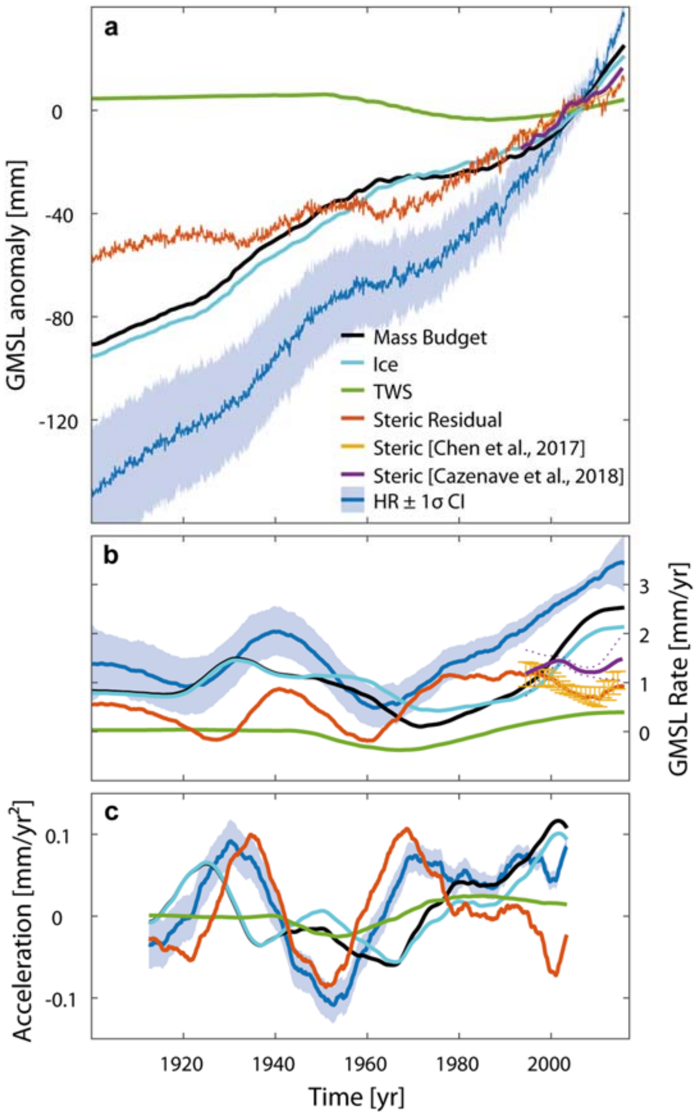

Fig. S9 | GMSL acceleration and the contribution of mass loss and thermal expansion. a, GMSL from the HR, a recent estimate of 20th century mass loss from glaciers[42], the two ice-sheets in Greenland[43] and Antarctica[40], terrestrial water storage (TWS)[40], and the steric residual resulting from the difference between the hybrid GMSL reconstruction and the sum of the individual contributions. The steric residual is validated with two independent estimates from temperature data from ref. 3 and ref. 1 over the altimetry period. All time series are plotted as anomalies relative to the 1993-2015 period. **b,** The corresponding rates inferred from a Singular System Analysis (SSA) with an embedding dimension of 10 years. The error bars and dotted lines correspond to the 1σ uncertainties from the steric components, respectively. **c,** 25-yr moving acceleration coefficients.

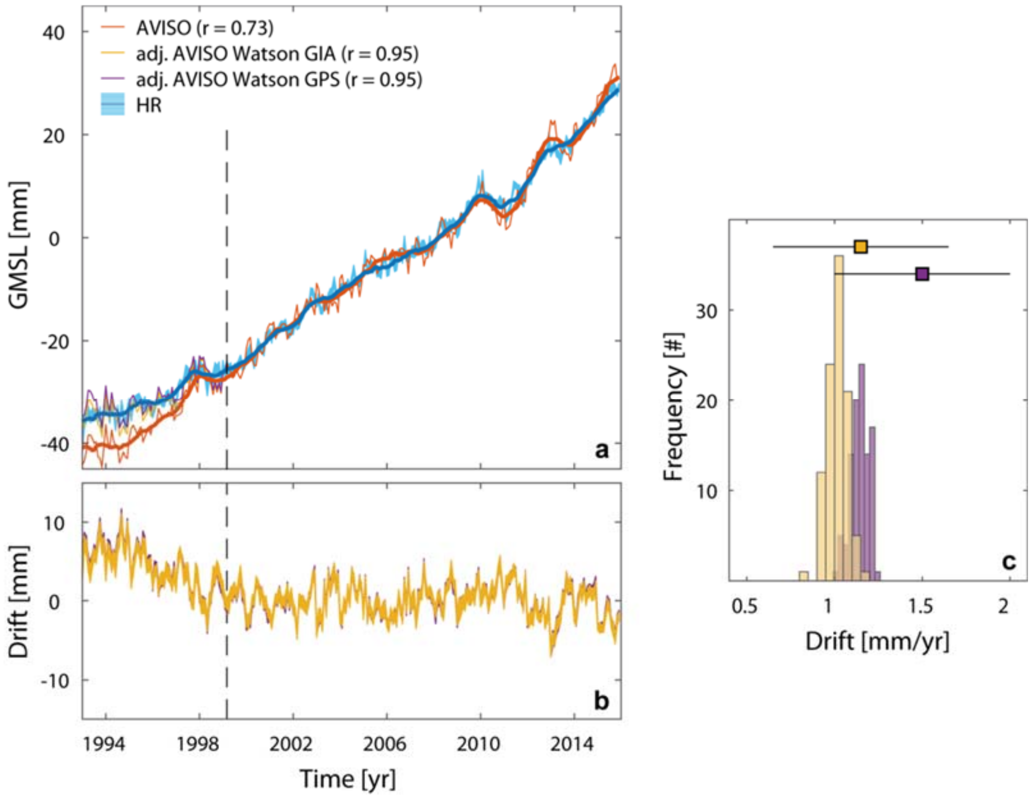

Fig. S10 | GMSL from the HR and satellite altimetry during 1993-2015. a Time series of GMSL from the HR (cyan = ensemble from 500 randomly selected tide gauge subsets, each consisting of either 80, 160, 240, 320, or 400 records; blue = HR) and AVISO satellite altimetry. Shown is the original altimeter record (red line) as well as two series with the lower/upper TOPEX Poseidon drift corrections from ref. 60 and their correlations with the HR. **b** Drift estimates from the differences between GMSL from the HR and uncorrected AVISO satellite altimetry based on all 500 ensemble members applying either the GIA-based (yellow, 1.1 mm yr^{-1}) or the GPS-based (magenta, 1.5 mm yr^{-1}) drift correction from ref. 60 before calculating EOFs. **c** Histograms of the trend differences between the HR and AVISO satellite altimetry for the period January 1993 to February 1999. The two GIA-based (yellow) and GPS-based (magenta) from ref. 60 are shown as colored boxes with 2σ error bars.

Supplementary References

1. Meyssignac, B. et al. Evaluating Model Simulations of Twentieth-Century Sea-Level Rise. Part II: Regional Sea-Level Changes. *J. Climate*, **30**, 8565-8593 (2017).